



Copper nanoparticle-decorated nitrogen-doped carbon nanosheets for electrochemical determination of paraquat

Jie Zhou^{1,2} · Zongshan Zhao¹ · Xue Zhao² · Sam Toan³ · Lei Wang³ · Thomas Wågberg⁴ · Guangzhi Hu²

Received: 19 February 2023 / Accepted: 21 April 2023 / Published online: 7 June 2023
© The Author(s), under exclusive licence to Springer-Verlag GmbH Austria, part of Springer Nature 2023

Abstract

A new strategy to prepare copper (Cu) nanoparticles anchored in nitrogen-doped carbon nanosheets (Cu@CN) has been designed and the nanomaterial applied to the determination of paraquat (PQ). The nanocomposite materials were characterized by transmission electron microscopy (TEM), X-ray diffraction (XRD), X-ray photoelectron spectroscopy (XPS), and several other techniques. We found that the Cu nanoparticles are uniformly distributed on the carbon materials, providing abundant active sites for electrochemical detection. The electrochemical behavior of the Cu@CN-based PQ sensor was investigated by square-wave voltammetry (SWV). Cu@CN exhibited excellent electrochemical activity and PQ detection performance. The Cu@CN-modified glassy carbon electrode (Cu@CN/GCE) exhibited excellent stability, favorable sensitivity, and high selectivity under optimized conditions (enrichment voltage -0.1 V and enrichment time 400 s) of the SWV test. The detection range reached 0.50 nM to 12.00 μ M, and the limit of detection was 0.43 nM with high sensitivity of 18 μ A $\cdot\mu$ M⁻¹ \cdot cm⁻². The detection limit is 9 times better than that of the high-performance liquid chromatography method. The Cu@CN electrochemical sensor demonstrated excellent sensitivity and selectivity also in environmental water and fruit samples enabling its use in practical, rapid trace-level detection of PQ in environmental samples.

Keywords Nitrogen-doped carbon nanosheets · Copper nanoparticles · Paraquat · Food analysis · Square-wave voltammetry

Introduction

Paraquat (PQ), also referred to as 1,1'-dimethyl-4,4'-bipyridinium, is a quick acting, broad spectrum, touch-killing, biocide herbicide that is commonly used in agriculture

to remove broadleaf weeds [1]. Paraquat is commonly used for weeding in orchards, rubber plantations, rice fields, and dry land. However, PQ is highly toxic to humans and animals and can damage the liver, heart, lungs, and kidneys while also known to cause Parkinson's disease [2]. Currently, the maximum allowable residue limits for PQ in different countries are around 40–400 nM, and there is no cure or medical treatment for PQ poisoning. The presence of PQ is very persistence following contact with soil and is highly soluble in water (620 g \cdot L⁻¹ 25 °C), enabling it to remain in the environment and cause widespread contamination [3]. Although PQ has been banned in the European Union and other countries, it is still widely used in more than 100 other countries, killing many people due to paraquat poisoning every year [4]. Therefore, it is crucial to develop an efficient and rapid PQ detection method.

There are numerous methods for the detection of paraquat, such as fluorescence [5], colorimetry [6], liquid chromatography–tandem mass spectrometry [7], and surface-enhanced Raman scattering (SERS) [8, 9]. The various methods mentioned above can accurately determine the content of paraquat,

✉ Zongshan Zhao
zhaozs@qdu.edu.cn

✉ Lei Wang
wan00818@umn.edu

✉ Guangzhi Hu
guangzhihu@ynu.edu.cn

¹ College of Environmental Science and Engineering, Qingdao University, Qingdao 266071, China

² Institute for Ecological Research and Pollution Control of Plateau Lakes, School of Ecology and Environmental Science, Yunnan University, Kunming 650504, China

³ Department of Chemical Engineering, University of Minnesota-Duluth, Duluth, MN 55812, USA

⁴ Department of Physics, Umeå University, 90187 Umeå, Sweden

though they often require complex pretreatment of samples, extensive instrumentation, and time-consuming procedures. Electrochemical methods can detect pollutants in various environments owing to its portability, rapid detection ability, high selectivity, and sensitivity [10–13]. The performance of a sensor platform depends on its favorable conductivity and abundant accessible active sites. Nanomaterial-modified electrodes exhibit excellent electrochemical performance. Using carbon or polymers as support of metallic nanoparticles to increase sensor's conductivity has been proven to be a success strategy [14–18]. For example, a self-assembled Bi film and Au nanoparticle-modified screen-printed carbon electrode (SPCE) (Bi/AuNP-SPCE) has been prepared for detecting low levels of Zn(II), Pb(II), and Cu(II) [15]. Beyond that, electrochemical methods based on these materials have also been used to detect PQ as an efficient and easy-to-operate alternative method [19–22]. Rajaram et al. synthesized Au nanoparticle-incorporated multiwalled carbon nanotubes for the electrochemical detection of PQ with limit of detection (LOD) of 32.00 nM [23]. Xiong et al. used the signal enhancement effects of gold nanoparticles (Au NPs) to improve the selectivity and sensitivity on PQ detection [24] and reached detection limit as low as 0.034 nM when using the CP[5]-Au NPs (3 nm)-modified nano-sensor. Zhang et al. built a ternary nanocomposite film electrode based on MoS₂ and Au nanoparticles to functionalize boron nitride for the determination of PQ with 0.074 μM LOD [25].

Non-noble metals such as Cu have been used as low-cost alternatives; their favorable redox ability makes them good candidates for the modification of electrodes [26, 27]. However, the sintering of Cu on the surface of the carbon decreases the catalyst active sites [28]. Dmitri et al. demonstrated that N-doping could resolve the sintering of Cu nanoparticles on the supported carbon to improve the performance of the catalytic materials [29]. N-doping of carbon adjusts the electronic structure of the space charge layer to form highly reactive graphitic N sites in the electrochemical reaction [29].

In this work, Cu@CN nanosheets were fabricated using a simple method for PQ detection. The performance for detecting PQ was tested and evaluated in real water environments (lake water, tap water, and cabbage-rinsed water), fruit samples (lemon juice), and vegetable samples (cabbage juice), including determination of linear relationships and recovery rates. The proposed method provides a novel electrochemical detection system for efficient, rapid, and accurate trace-level detection of PQ.

Experimental

Materials and reagents

Ultrapure water (resistance $\geq 18.25 \text{ M}\Omega \text{ cm}^{-1}$), prepared with Milli-Q purification equipment (Milli-Q USA), was

used to prepare all solutions used in this experiment. 1,10-Phenanthroline (C₁₂H₈N₂·H₂O, 99%), zinc nitrate (Zn(NO₃)₂·6H₂O, 98%), copper(II) nitrate (Cu(NO₃)₂·3H₂O, 99%), dibasic sodium phosphate (Na₂HPO₄, 99%), sodium dihydrogen phosphate (NaH₂PO₄, 99%), sodium chloride (NaCl, 99.5%), and PQ (99.7%) were obtained from Macklin (Shanghai, China). Lake water samples were taken from Ze Lake (Kunming, China), and tap water samples were obtained from the living building from Yunnan University in Kunming China. Lemon and cabbage were purchased from a local market. All the reagents were analytically pure and could be used directly.

Preparation of Cu@CN nanosheets and N-doped carbon

Cu@CN nanosheets and N-doped carbon (CN) were synthesized through simple pretreatment and subsequent thermal treatment. This method is simply modified from the previous reference [30]. The specific synthesis process was in the supporting information.

Characterization of Cu@CN

The Cu@CN nanoparticles were characterized by scanning electron microscopy (SEM), transmission electron microscopy (TEM), Fourier transform infrared (FTIR) spectroscopy, Raman spectra, X-ray diffraction (XRD), and X-ray photoelectron spectroscopy (XPS). The specific instrument models were in the support information.

Preparation of Cu@CN/GCE

The treatments for the bare glassy carbon electrodes (GCE) were detailed in the supporting information. The Cu@CN powder was dispersed in ultrapure water, N, N-dimethylformamide (DMF), and Nafion (5:4.5:0.5); 5 μL Cu@CN ink (1 mg mL⁻¹) was then added to the electrode surface. The mixture was allowed to stand for 24 h at room temperature until the ink was completely evaporated.

Electrochemical measurements

Electrochemical measurements were performed using a CHI 660E electrochemical workstation (Shanghai Chenhua Instrument Co. Ltd., Shanghai, China). 0.1 M phosphate-buffered solution (PBS) was used as electrolyte solution for electrochemical experiment. The measurements were performed using a three-electrode system; the detailed performances were listed in the supporting information. The scanning rate of linear sweep voltammetry (LSV) tests ($n =$

3) was performed from -0.9 to -0.3 V at the scanning rate in a range of 10 – 200 $\text{mV}\cdot\text{s}^{-1}$. The cyclic voltammetry (CV) tests were performed from -0.9 to -0.3 V at the scanning rate of 100 $\text{mV}\cdot\text{s}^{-1}$. The PQ detection was performed via SWV method ($n = 3$) at -0.1 V (enrichment voltage) and 400 s (enrichment time) in 0.1 M PBS (50 mL, pH 7). The peak potential of PQ detection was obtained at -0.65 V.

Preparation of real samples

The real water samples filtered through a 0.45 - μm membrane were directly diluted with PBS (0.1 M) at a ratio of $1:1$. Lemons were chosen as the fruit sample, and cabbages were selected as the vegetable sample. The lemon and cabbage juice were filtered through a 0.45 - μm membrane. The lemon and cabbage juice were diluted with PBS (0.1 M) at a ratio of $19:1$. Real water samples and lemon and cabbage juice samples containing different concentrations of PQ were analyzed by SWV method.

High-performance liquid chromatography (HPLC) was used to compare the accuracy of the Cu@CN-based sensor detection of PQ. The real samples were all filtered through

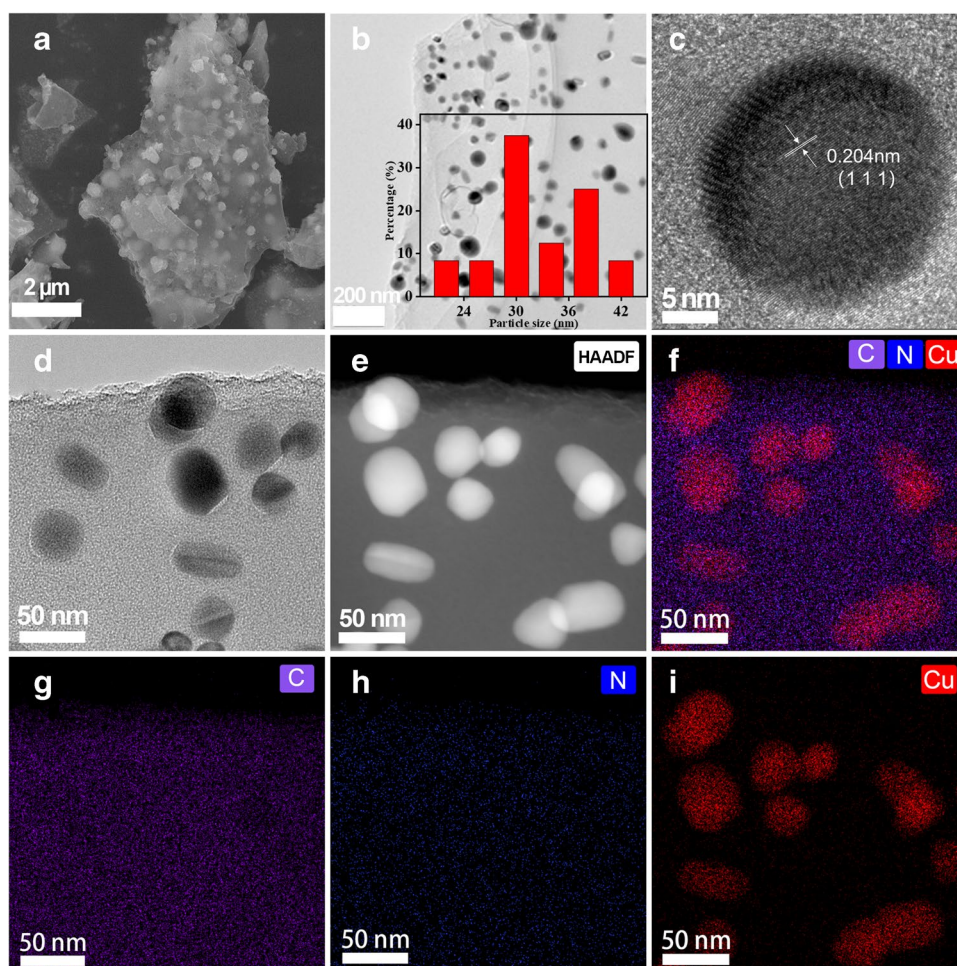
0.22 - μm nylon membrane. The standard curve was established for the detection of the prefabricated solution (3 , 50 , 150 , 400 , 600 nM); bare and spiked real samples were analyzed by HPLC (mobile phase: acetonitrile/water; $60\%:40\%$; injection rate: $1\text{mL}\cdot\text{L}^{-1}$; injection volume: 20 μL) [31].

Results and discussion

Characterization of Cu@CN

The SEM image of Cu@CN was shown in Fig. 1a; round Cu particles were grown on the carbon sheets. From the TEM image of Cu@CN, the Cu nanoparticles were found to be embedded on the nanosheets. It can be seen from Fig. 1b that the particle size distribution of the Cu nanoparticles lies mainly in the range of 32.00 – 38.00 nm, while the average particle size was 32.40 nm. Uniformly sized nanoparticles evenly distributed in the carbon materials provided abundant active sites. At the same time, as shown in the TEM image in Fig. 1c of the enlarged Cu particles, the observed lattice fringes of 0.204 nm correspond to the face-centered cubic

Fig. 1 a SEM images of Cu@CN; b TEM images of Cu@CN; inset shows the Cu particle size distribution graph; c and d HRTEM images of Cu@CN; e–i elemental mapping images of Cu, C, and N in Cu@CN



structure of the upper Cu [32]. According to Fig. 1f–i, it can be seen from the energy dispersive spectrum that C and N are uniformly distributed, while Cu is concentrated on the spherical particles. In addition, Cu is distributed in the carbon material in the form of nanoparticles.

From Fig. 2c, the XRD pattern shows that the four peaks identified in the PDF standard card (#01-1241) of Cu of the Committee for Powder Diffraction Standards (JSPDS) correspond to 43.47, 50.37, 73.99, and 89.93°, respectively [32], which are consistent with the (111), (200), (220), and (311) crystal planes; the weak peak before 43.47° corresponds to the peak of the CuO standard card (#45-9537) [33]. Cu primarily exists in the material in the zero-valence state while also present in the form of Cu²⁺.

In Fig. 2d, the high-resolution Cu 2p core-level spectra of Cu@CN correspond to Cu 2p_{3/2} and Cu 2p_{1/2}, confirming the presence of Cu⁰/Cu²⁺, along with the presence of two satellite peaks at 941.2 and 962.45 eV [34, 35]. The Cu 2p_{1/2} and Cu 2p_{3/2} spectra resolved into three peaks. The Cu 2p_{3/2} at 932.65 eV and Cu 2p_{1/2} at 952.55 eV could be attributed to Cu⁰; meanwhile, the Cu 2p_{3/2} at 933.8 and 935.2 eV and Cu 2p_{1/2} at 954 and 954.9 eV were due to Cu²⁺. The XRD results obtained demonstrate the presence of Cu and CuO species. CuO could be attributed to the oxidation of the material in air. The high-resolution C 1s spectrum of Cu@CN in Fig. 2e displays four representative peaks that could be attributed to the C–C (284.8 eV), C–N (285 eV), C=C (286 eV), and C=N (287.5 eV) bonds, respectively [36]. The high-resolution N 1s spectra

Fig. 2 **a** Raman spectroscopy of Cu@CN; **b** FTIR spectra of Cu@CN and CN; **c** XRD image of Cu@CN; **d–f** XPS spectra of Cu, C, and N in Cu@CN

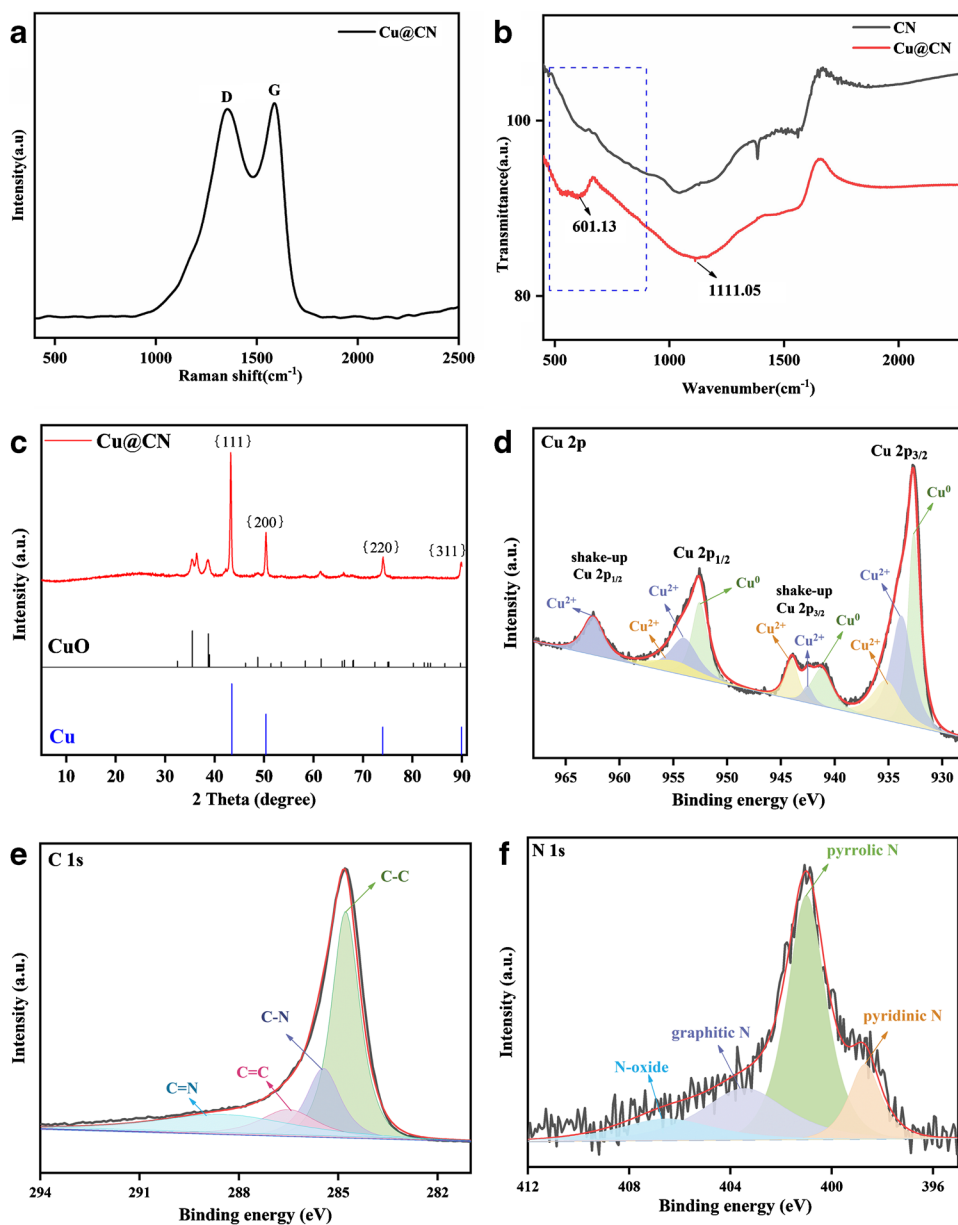


(Fig. 2f) were fitted to three peaks at 398.69 eV (pyridinic N), 401 eV (pyrrole N), 403.45 eV (graphitic N) and 406.53 eV (N-oxide)[37].

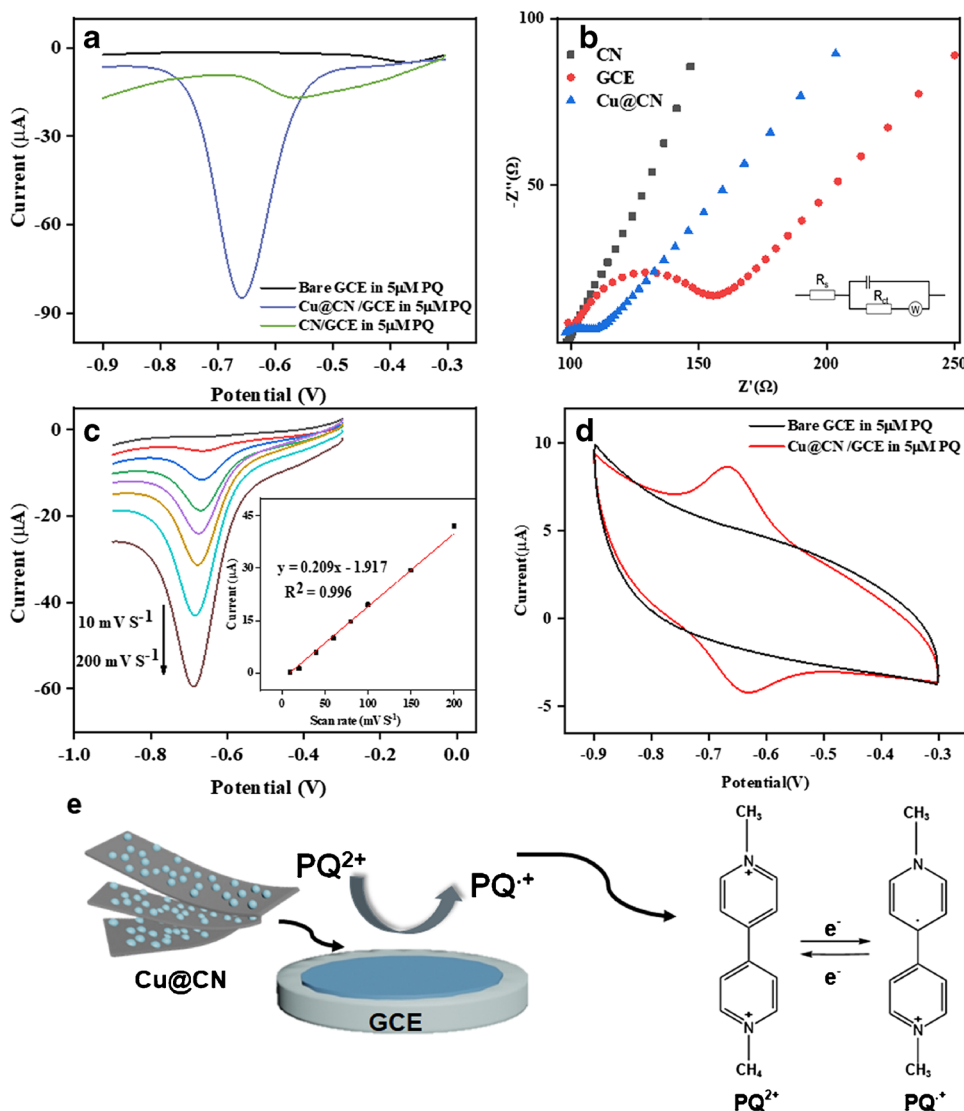
In Fig. 2a, D peak at 1354.36 cm^{-1} and G peak at 1586.63 cm^{-1} in the Raman spectra of Cu@CN correspond to the distortion of lattice, indicating the defect of the carbon structure and the introduction of N into the carbon structure [38]. Compared with the FTIR spectra of CN with black line in Fig. 2b, the peak at around 601.13 cm^{-1} in the red line of Cu@CN confirmed that the Cu species was successfully introduced into the carbon materials. Meanwhile, the peak at 1111.05 cm^{-1} could be attributed to the vibration of Cu-N [39].

Electrochemical performance of Cu@CN/GCE

SWV tests were performed to compare the PQ detection performance of the electrodes [40]. The 5 μM PQ was added

to a PBS (pH 7) to facilitate the testing of the Cu@CN/GCE, CN/GCE, and bare GCE electrodes. The deposition time was 400 s, and the deposition potential was -0.1 V for the $i-t$ curve. As shown in Fig. 3a, Cu@CN/GCE exhibits the most favorable response current. The current response intensity of Cu@CN/GCE to PQ was significantly higher than that of the CN/GCE modified electrode and bare electrode; a higher current response occurred on the Cu@CN-modified surface, indicating that the doping of Cu plays an important role in the reduction reaction of PQ. Catalytic performance correlates with improved conductivity for the reduction reaction on the Cu@CN/GCE surface. The uniform distribution of Cu nanoparticles on the electrode surface increased the number of reaction sites on the Cu@CN/GCE surface, resulting in a large step enhancement of the electrical signal. Nyquist plot (EIS) was used to evaluate the modified electrodes' charge transfer characteristics, and the semicircle diameter in Fig. 3b represents the charge transfer resistance

Fig. 3 **a** SWV response of Cu@CN/GCE, CN/GCE, and bare electrode to 5 μM PQ; **b** Nyquist plot (EIS) of Cu@CN/GCE, CN/GCE, and GCE in 0.1 M KCl solution containing 5 mM $[\text{Fe}(\text{CN})_6]^{3-/4-}$, with frequency range of 10^{-1} – 10^7 Hz and amplitude of 0.1 V_{RMS} ; **c** LSV curves of Cu@CN at varying scan rates with an inset showing the linear fit of the scan rate and the current intensity response; **d** CV spectra of Cu@CN/GCE in 5 μM PQ; **e** detection mechanism of Cu@CN/GCE ($n=3$)



(R_{ct}) where smaller diameter means that the electrodes have smaller R_{ct} and higher charge conductivity [41]. As shown in Fig. 3b, the R_{ct} order of Cu@CN (10.6 Ω) < GCE (42.0 Ω) < CN (558.3 Ω) verifies the conclusions obtained from Fig. 3a.

The control mechanism for substance detection on the electrode surface was analyzed using LSV curves obtained at varying scanning rates. The detection of contaminants on the electrode surface may be adsorption- or diffusion-controlled. As shown in Fig. 3c, the current response intensity increased with an increase in the scan rate. As shown in Fig. 3c, the scan rate and current intensity exhibited an excellent linear relationship and were positively correlated. This indicates that the adsorption process dominated the reaction on the surface of the electrode

CV spectra of Cu@CN/GCE in 5 μ M PQ were shown in Fig. 3d. A reduction peak and an oxidation peak in symmetrical distribution correspond to the rounded redox reaction of PQ. The reduction mechanism (Fig. 3e) can be classified as a charge transfer process of single-electron reduction to +2-valent PQ dicationic ions, forming cationic radicals [19, 42]. The chemical equation used is $PQ^{2+} + 1e^- \rightleftharpoons PQ^{*+}$. According to the results, the redox peak with a current response of -0.66 V was chosen as the target peak to detect PQ [43].

Experimental condition optimization

To obtain the optimal PQ detection current, the effect on the electrical signal of the Cu@CN ink amount applied towards electrode modification, enrichment voltage, enrichment time, and pH was explored. Fig. S1 (a) shows that 1 mg·mL⁻¹ was the most suitable concentration to obtain the highest current response, as high levels of modified electrode material will hinder the efficiency of electron transfer. The effects of pH value on the electrical signal of paraquat were carried out in pH gradients from 5 to 9. The results indicate that the highest signals can be obtained at neutral conditions (Fig. S1 (b)). Usually, PQ can decompose under excessively alkaline conditions, while, on the contrary, the generated protons on the surface of the electrolyte in acidic environments would hinder the PQ adsorption on the electrode surface. Fig. S1 (c) showed that the current signal presented the highest value when the enrichment voltage is set at -0.1 V, indicating that the reduction reaction of PQ takes place in this voltage range. From Fig. S1 (d), the increasing current with increased enrichment time as well as PQ was in consistent with the strong adsorption behavior. However, when the enrichment time exceeded 400 s, the growth amplitude of the current signal began to decrease. Therefore, an enrichment voltage of -0.1 V and enrichment time of 400 s was employed in the subsequent experiments.

Electrochemical detection of PQ and linear fit

PQ electrochemical detection was carried out under optimized conditions to obtain the SWV curves. Figure 4 shows the peak shape plots of the SWV current responses for different PQ (0.5 nM to 12 μ M), while Fig. 4 shows the corresponding linear relationship. The peak value of SWV increased continuously with increasing PQ concentration. The linear regression equation is $I(\mu A) = 0.0180 C$ (PQ/nmol·L⁻¹) + 0.0996 ($R^2 = 0.998$). The sensitivity of PQ was 18 $\mu A \cdot \mu M^{-1} \cdot cm^{-2}$ in the concentration range from 0.50 nM to 12.00 μ M. The LOD was 0.43 nmol/L, which was calculated using the formula $LOD = 3S_b/S$. S_b is the standard deviation of the 10-fold blank solution detection current, and S is the slope of the calibration curve.

The prepared electrode was compared with other modified electrodes from other reports, and the detailed information were listed in the Table 1. According to Table 1, the Cu@CN/GCE electrode showed a relatively LOD and compared or better linear range, indicating that the Cu@CN/GCE could be used in the PQ trace-level detection.

Stability and selectivity studies

Two sets of experiments were performed to explore the repeatability and reproducibility of the electrodes. Five micrometer of PQ was added to a 0.1 M PBS, while detection was consistent with the SWV curve; the same electrode was used for detection in 20 consecutive instances. This test was repeated for the five electrodes. As shown in Fig. 5a, the current did not alter significantly following 25 measurements; the relative standard deviation (RSD) was only 0.11%. Moreover, as shown in Fig. 5b, the RSD of the

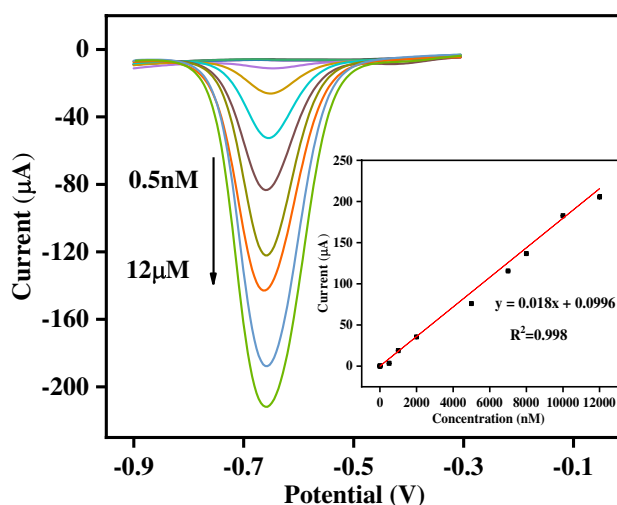


Fig. 4 SWV response of Cu@CN/GCE at different PQ concentrations; inset shows the linear fit of current intensity and the PQ concentration ($n=3$)

Table 1 Electrochemical performance comparison of the Cu@CN sensor to the other PQ sensors

Electrode	Technique	Linear range (μM)	LOD (nM)	Ref.
PPY-g-NGE/GCE ^a	DPV	0.050–2.00	58.00	[44]
CP5-AgNPs/GO/GCE ^b	DPV	0.010–10.00	10.00	[43]
rGO-AB4 ^c	AdDPSV	0.70–9.80	23.10	[42]
BN/MoS ₂ /AuNPs/GCE ^d	DPV	0.10–100.00	74.00	[25]
Fe ₂ O ₃ -MIL-100/GCE ^e	SWV	0.010–30.00	2.60	[41]
Cu@CN/GCE	SWV	0.00050–12.00	0.43	This work

^aPolypyrrole-grafted nitrogen-doped graphene-modified glassy carbon electrode; ^bcarboxylated pillar[5] arene-modified silver nanoparticle-anchored graphene oxide-modified glassy carbon electrode; ^cactivated biochar and reduced graphene oxide-modified electrodes; ^dmolybdenum disulfide and gold nanoparticle-functionalized boron nitride-modified glassy carbon electrode; ^eMIL-100(Fe) loaded with iron oxide-modified glassy carbon electrode

five electrodes is 0.78%, which proves that the modified electrodes possess a high reproducibility. From the above experiments, the Cu@CN material was shown to exhibit favorable repeatability, reproducibility, and stability. As shown in Fig. 5c, the signal response of the electrodes on the first, fifth, tenth, and fifteenth days did not change significantly and remained quite stable. The fifteenth day's current intensity only dropped by 5.9% relative to the first day's response. Subsequently, the anti-interference effect of the electrodes could be studied. Five micrometer of PQ was added to a 0.1 M PBS, while organic and inorganic ions were added at concentrations 100 times higher than that of PQ including Na⁺, Ca²⁺, Cl⁻, Mg²⁺, Zn²⁺, K⁺, CO₃²⁻, HCO₃⁻, and SO₄²⁻, as well as small molecules such as ascorbic acid (AS), sodium citrate (SOD

CITR), and glucose (GLU). To further investigate the anti-interference ability of Cu@CN-modified electrode, other potential interference organic compounds like atrazine (AT), glyphosate (GLY), glufosinate-amomonium (GLU-A), butachlor, and propanil were added. As shown in Fig. 5d, the current signal dropped slightly, possibly owing to the adsorption and subsequent occupation of the active sites on the surface of the electrode owing to AT, GLU-A, GLY, and butachlor. The current of Zn²⁺ decreased due to the deposition of Zn²⁺, which may have affected the adsorption of PQ, while HCO₃⁻ and CO₃²⁻ also decreased the current of the PQ signal by influencing the pH of the electrolyte. However, the influence of these ions and small molecules was relatively insignificant, proving that the electrode possesses favorable selectivity for PQ.

Fig. 5 **a** Repeatability of response of Cu@CN/GCE in 25 measurements; **b** reproducibility of response of Cu@CN/GCE using 5 different electrodes; **c** stability of Cu@CN/GCE over 15 days; **d** SWV test on the detection of PQ with the presence of interfering materials (*n*=5)

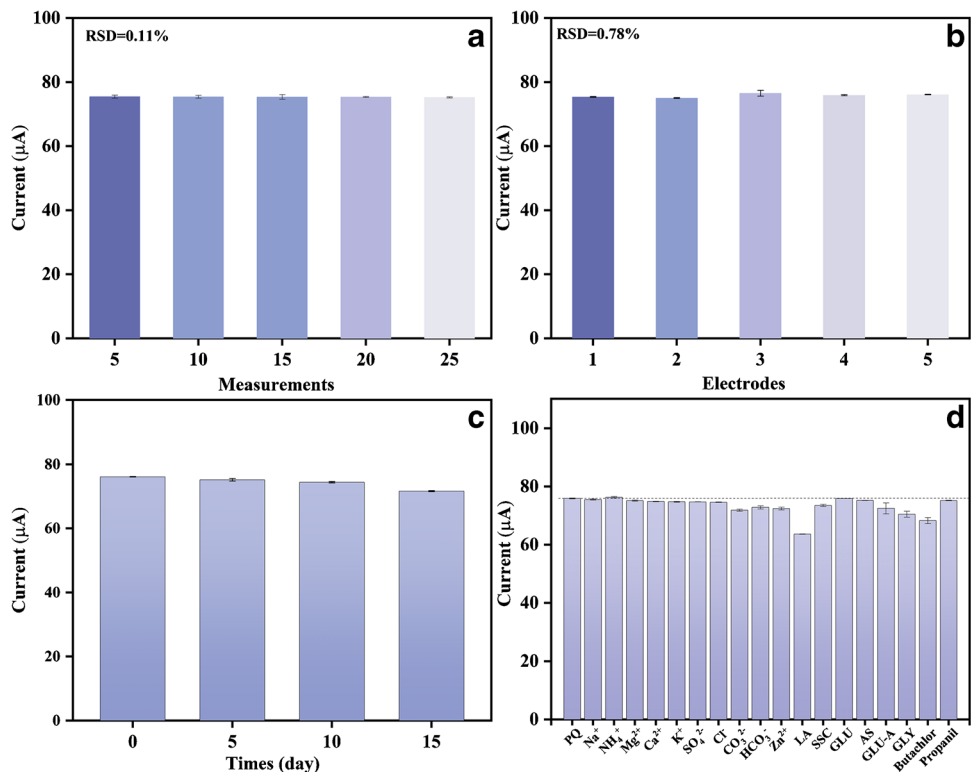


Table 2 Analytical results of the detection of PQ in real samples using SWV tests ($n = 3$)

Real sample	Added amount (nM)	Found amount (nM)	Recover rate (%)	RSD (%)	HPLC (nM)	RSD (%) of HPLC
Lake water	100.0	97.8	97.8	1.6	103.1	1.6
	200.0	195.7	97.9	1.6	197.8	1.1
Tap water	100.0	99.3	99.3	1.8	102.7	1.2
	200.0	201.4	100.7	2.2	201.1	1.0
Cabbage-rinsed water	100.0	104.6	104.6	1.4	104.3	0.9
	200.0	202.8	101.4	0.9	198.6	0.9
Cabbage	100.0	102.3	102.3	0.6	102.6	1.4
	200.0	195.4	97.7	0.8	201.6	0.9
Lemon juice	8.0	7.9	98.3	1.4	7.7	1.0
	20.0	20.6	103.0	0.6	20.7	1.2

Analysis of the real sample

The practicability of Cu@CN/GCE was further explored by detecting PQ in lake water, tap water, vegetable-rinsed water, and fruit and vegetable samples. Linear fits were obtained using the SWV test detection of the PQ. The original concentration of PQ was below the detection limits in the real non-spiked samples. By introducing different amounts of PQ into these samples, the obtained recovery rate was obtained and is presented in Table 2. The amount of PQ added to the lake and tap water, cabbage-rinsed water, and cabbage juice was 100.0 and 200.0 nM, respectively. The spiked recoveries measured for the lake water, tap water, cabbage-rinsed water, and cabbage and lemon juice samples were in the range of 97.7 % and 104.6 %. The results were comparable to that obtained using HPLC (96.3–104.3 %; RSD: 0.9–1.6 %). Totally, the Cu@CN/CGE showed a satisfying sensitive and stable PQ detection performance. The maximum contaminant level for PQ in drinking water is 0.7 μ M according to the US Environmental Protection Agency (EPA) [45]. The LOD of the lemon juice, cabbage juice, cabbage-rinsed water, tap water, and lake water were 1.8 nM, 27.3 nM, 25.5 nM, 8.7 nM, and 11.8 nM, respectively, which were lower than the Chinese standard of the PQ maximum residue in food (0.78 μ M) [46]. The RSD was approximately 0.6–2.2 %, indicating that the relative errors were low and that the results of the real sample tests were accurate. The detection limits of Cu@CN/GCE were lower than the maximum allowable residue limits in environment indicates that the Cu@CN electrode can be applied in real situation applications.

Conclusion

The as-prepared Cu@CN demonstrated a favorable signal response for PQ in the PBS electrolyte relative to the bare and CN-modified electrodes in the context of the SWV

method. The introduction of Cu enhanced the electrical conductivity of N-doped carbon and increased the number of active sites for PQ detection. The current signal dropped slightly in the presence of other herbicide targets with chemical structures similar to PQ. The prepared electrode also presented a high accuracy and stability performance when analyzing actual environmental samples, indicating its potential for detecting trace-level of PQ with simple sample-pretreatment.

Supplementary Information The online version contains supplementary material available at <https://doi.org/10.1007/s00604-023-05812-0>.

Author contributions Jie Zhou performed experiments, carried out the sample characterization and data analysis, and wrote the manuscript draft. Xue Zhao, Sam Toan, Baoling Wang, Xiujun Deng, and Thomas Wägberg, assisted with the investigation, methodology, data discussion, and formal analysis. Zongshan Zhao, Lei Wang, and Guangzhi Hu co-guided the conceptional idea, resources, financial support, and review, editing manuscript.

Funding This work was supported by the National Key R&D Program of China (2019YFC1804400) and Double-First Class University Plan (C176220100042).

Declarations

Competing interests The authors declare no competing interests.

Conflict of interest The authors declare that they have no competing of interests.

References

- Halfon E, Galassi S, Bruggemann R, Provini A (1996) Selection of priority properties to assess environmental hazard of pesticides. *Chemosphere* 33:1543–1562. [https://doi.org/10.1016/0045-6535\(96\)00274-3](https://doi.org/10.1016/0045-6535(96)00274-3)
- Weed LD (2021) Does paraquat cause Parkinson's disease? A review of reviews. *Neurotoxicology* 86:180–184. <https://doi.org/10.1016/j.neuro.2021.08.006>

3. Zhao Z, Zhang F, Zhang Z (2018) A facile fluorescent “turn-off” method for sensing paraquat based on pyranine-paraquat interaction. *Spectrochim Acta Part a-Mol Biomol Spectrosc* 199:96–101. <https://doi.org/10.1016/j.saa.2018.03.042>
4. Hamilton DJ, Ambrus A, Dieterle RM, Felsot AS, Harris CA, Holland PT, Katayama A, Kurihara N, Linders J, Unsworth J, Wong SS (2003) Regulatory limits for pesticide residues in water - (IUPAC Technical Report). *Pure Appl Chem* 75:1123–1155. <https://doi.org/10.1351/pac200375081123>
5. Luo Y, Zhang W, Liu M, Zhao J, Fan Y, Bian B, Tao Z, Xiao X (2021) A supramolecular fluorescent probe based on cucurbit 10 uril for sensing the pesticide dodine. *Chin Chem Lett* 32:367–370. <https://doi.org/10.1016/j.ccllet.2020.02.023>
6. Kuitio C, Klangprapan S, Chingkiti N, Boonthavivudhi S, Choowongkamon K (2021) Aptasensor for paraquat detection by gold nanoparticle colorimetric method. *J Environ Sci Heal* 56:370–377. <https://doi.org/10.1080/03601234.2021.1888615>
7. Oulkar D, Shinde R, Khan Z, Banerjee K (2019) High throughput residue analysis of paraquat and diquat involving hydrophilic interaction liquid chromatographic separation and mass spectrometric determination. *Food Addit Contam Part A* 36:120–130. <https://doi.org/10.1080/19440049.2018.1547424>
8. Zhu C, Liu D, Yan M, Xu G, Zhai H, Luo J, Wang G, Jiang D, Yuan Y (2022) Three-dimensional surface-enhanced Raman scattering substrates constructed by integrating template-assisted electrodeposition and post-growth of silver nanoparticles. *J Colloid Interface Sci* 608:2111–2119. <https://doi.org/10.1016/j.jcis.2021.10.133>
9. Li Q, Du Y, Wang X, Cao P, Sui T, Xu Y, Geng J (2013) Rapid atto-molar level detection of surface-enhanced Raman spectroscopy technique based on glycidyl methacrylate-ethylene dimethacrylate (GMA-EDMA) porous material. *J Raman Spectrosc* 44:1004–1009. <https://doi.org/10.1002/jrs.4322>
10. Khosropour H, Kalambate PK, Kalambate RP, Permpoka K, Zhou X, Chen GY, Laiwattanapaisal W (2022) A comprehensive review on electrochemical and optical aptasensors for organophosphorus pesticides. *Microchim Acta* 189. <https://doi.org/10.1007/s00604-022-05399-y>
11. Kokulnathan T, Wang T-J, Wang Y-Y, Suvina V, Ahmed F (2022) Three-dimensional manganese cobaltate: a highly conductive electrocatalyst for paraoxon-ethyl detection. *Microchim Acta* 189. <https://doi.org/10.1007/s00604-022-05416-0>
12. Wachholz Junior D, Deroco PB, Kubota LT (2022) A copper-based metal-organic framework/reduced graphene oxide-modified electrode for electrochemical detection of paraquat. *Microchim Acta* 189. <https://doi.org/10.1007/s00604-022-05358-7>
13. Wan Y, Wang H, Zhang L, Chen Y, Li S, Zhou J, Zhang Q, Xia L (2022) Highly stable acetylcholinesterase electrochemical biosensor based on polymerized ionic liquids microgel for pesticides detection. *Microchim Acta* 189. <https://doi.org/10.1007/s00604-022-05383-6>
14. Chemchoub S, El Attar A, Oularbi L, Younssi SA, Bentiss F, Jama C, El Rhazi M (2022) Electrosynthesis of eco-friendly electrocatalyst based nickel-copper bimetallic nanoparticles supported on poly-phenylenediamine with highest current density and early ethanol oxidation onset potential. *Int J Hydrogen Energ* 47:39081–39096. <https://doi.org/10.1016/j.ijhydene.2022.09.069>
15. Lu Z, Zhang J, Dai W, Lin X, Ye J, Ye J (2017) A screen-printed carbon electrode modified with a bismuth film and gold nanoparticles for simultaneous stripping voltammetric determination of Zn(II), Pb(II) and Cu(II). *Microchim. Acta* 184:4731–4740. <https://doi.org/10.1007/s00604-017-2521-8>
16. Mouratib R, Oularbi L, Achargui N, El Krati M, Younssi SA, Tahiri S, El Rhazi M (2022) Carbon paste electrode modified with Al- and Si-rich water treatment sludge for Bisphenol-A detection. *J Environ Chem Eng* 10. <https://doi.org/10.1016/j.jece.2022.108072>
17. Oularbi L, Turmine M, El Rhazi M (2019) Preparation of novel nanocomposite consisting of bismuth particles, polypyrrole and multi-walled carbon nanotubes for simultaneous voltammetric determination of cadmium(II) and lead(II). *Synthetic Met* 253:1–8. <https://doi.org/10.1016/j.synthmet.2019.04.011>
18. Oularbi L, Turmine M, Salih FE, El Rhazi M (2020) Ionic liquid/carbon nanofibers/bismuth particles novel hybrid nanocomposite for voltammetric sensing of heavy metals. *J Environ Chem Eng* 8. <https://doi.org/10.1016/j.jece.2020.103774>
19. de Oliveira UMF, Lichtig J, Masini JC (2004) Evaluation of a Nafion coated glassy carbon electrode for determination of paraquat by differential pulse voltammetry. *J Brazil Chem Soc* 15:735–741. <https://doi.org/10.1590/s0103-50532004000500020>
20. Feng R, Wang M, Qian J, He Q, Zhang M, Zhang J, Zhao H, Wang B (2022) Monoclonal antibody-based enzyme-linked immunosorbent assay and lateral flow immunoassay for the rapid screening of paraquat in adulterated herbicides. *Microchem J* 180. <https://doi.org/10.1016/j.microc.2022.107644>
21. Li M, Wang X, Zhu Y, Jia X, Zhang S, Wang H, Li Y, Hu G (2022) Fe₂O₃-decorated boron/nitrogen-co-doped carbon nanosheets as an electrochemical sensing platform for ultrasensitive determination of paraquat in natural water. *Chin Chem Lett* 34:107299. <https://doi.org/10.1016/j.ccllet.2022.03.022>
22. Maciel CC, Freitas ASM, Medradas JP, Ferreira M (2022) Simultaneous determination of catechol and paraquat using a flexible electrode of pbat and graphite modified with gold nanoparticles and copper phthalocyanine (g-PBAT/AuNP/CuTsPc) LbL film. *J Electrochem Soc* 169:027505. <https://doi.org/10.1149/1945-7111/ac4ff0>
23. Rajaram R, Gurusamy T, Ramanujam K, Neelakantan L (2022) Electrochemical determination of paraquat using gold nanoparticle incorporated multiwalled carbon nanotubes. *J Electrochem Soc* 169:047522. <https://doi.org/10.1149/1945-7111/ac5bae>
24. Xiong Y, Ma T, Zhang H, Qiu L, Chang S, Yang Y, Liang F (2022) Gold nanoparticle functionalized nanopipette sensors for electrochemical paraquat detection. *Microchim Acta* 189:251. <https://doi.org/10.1007/s00604-022-05348-9>
25. Zhang J, Lin Z, Qin Y, Li Y, Liu X, Li Q, Huang H (2019) Fabricated electrochemical sensory platform based on the boron nitride ternary nanocomposite film electrode for paraquat detection. *ACS Omega* 4:18398–18404. <https://doi.org/10.1021/acsomega.9b02658>
26. Liu J, Wang X, Ma F, Yang X, Liu Y, Zhang X, Guo S, Wang Z, Yang S, Zhao R (2022) Atomic copper(I)-carbon nitride as a peroxidase-mimic catalyst for high selective detection of perfluorooctane sulfonate. *Chem Eng J* 435:134966. <https://doi.org/10.1016/j.cej.2022.134966>
27. Gao X, Zheng M, Lv H, Zhang Y, Zhu M, Hou Y (2022) Ultra-high sensitive flexible sensor based on textured piezoelectric composites for preventing sports injuries. *Compos Sci Technol* 229. <https://doi.org/10.1016/j.compscitech.2022.109693>
28. Wang C, Kim J, Tang J, Kim M, Lim H, Malgras V, You J, Xu Q, Li J, Yamauchi Y (2020) New strategies for novel MOF-derived carbon materials based on nanoarchitectures. *Chem* 6:19–40. <https://doi.org/10.1016/j.chempr.2019.09.005>
29. Bulushev DA, Chuvilin AL, Sobolev VI, Stolyarova SG, Shubin YV, Asanov IP, Ishchenko AV, Magnani G, Riccò M, Okotrub AV, Bulusheva LG (2017) Copper on carbon materials: stabilization by nitrogen doping. *J Mater Chem A* 5:10574–10583. <https://doi.org/10.1039/c7ta02282d>
30. Zhao X, Hu G, Tan F, Zhang S, Wang X, Hu X, Kuklin AV, Baryshnikov GV, Ågren H, Zhou X, Zhang H (2021) Copper confined in vesicle-like BCN cavities promotes electrochemical reduction

- of nitrate to ammonia in water. *J Mater Chem A* 9:23675–23686. <https://doi.org/10.1039/d1ta05718a>
31. Halim N, Kuntom A, Shinde R, Banerjee K (2019) Determination of paraquat residues in palm oil by high-performance liquid chromatography with UV and tandem mass spectrometry. *Eur J Lipid Sci Tech* 121. <https://doi.org/10.1002/ejlt.201900092>
 32. Xie W, Yang T, Tian N, Liu X-H, Chen J (2022) Cu nanoparticles decorating N-doped erythrocyte-shaped carbon nanostructures for electrochemical CO₂ reduction. *Energ Fuel* 36:958–964. <https://doi.org/10.1021/acs.energyfuels.1c03823>
 33. Ye Q, Chen X, Yang J, Wu D, Ma J, Kong Y (2019) Fabrication of CuO nanoparticles-decorated 3D N-doped porous carbon as electrochemical sensing platform for the detection of Sudan I. *Food Chem* 287:375–381. <https://doi.org/10.1016/j.foodchem.2019.02.108>
 34. Moretti E, Lenarda M, Riello P, Storaro L, Talon A, Frattini R, Reyes-Carmona A, Jimenez-Lopez A, Rodriguez-Castellon E (2013) Influence of synthesis parameters on the performance of CeO₂-CuO and CeO₂-ZrO₂-CuO systems in the catalytic oxidation of CO in excess of hydrogen. *Appl Catal B Environ* 129:556–565. <https://doi.org/10.1016/j.apcatb.2012.10.009>
 35. Fan S, Gao C, Duan C, Zhang S, Zhang P, Yu L, Zhang Z (2022) Geometry effect of copper nanoparticles and nanowires on polyetheretherketone-matrix nanocomposites: thermal conductivity, dynamic mechanical properties and wear resistance. *Compos Sci Technol* 219. <https://doi.org/10.1016/j.compscitech.2021.109224>
 36. Ren S, Xu X, Hu K, Tian W, Duan X, Yi J, Wang S (2022) Structure-oriented conversions of plastics to carbon nanomaterials. *Carbon Res* 1. <https://doi.org/10.1007/s44246-022-00016-2>
 37. Hu Y, Tang C, Li H, Du A, Luo W, Wu M, Zhang H (2022) B-incorporated, N-doped hierarchically porous carbon nanosheets as anodes for boosted potassium storage capability. *Chin Chem Lett* 33:480–485. <https://doi.org/10.1016/j.ccllet.2021.06.063>
 38. Liang Q, Li Z, Yu X, Huang Z-H, Kang F, Yang Q-H (2015) Macroscopic 3D porous graphitic carbon nitride monolith for enhanced photocatalytic hydrogen evolution. *Adv Mater* 27:4634–4639. <https://doi.org/10.1002/adma.201502057>
 39. Wen X, Qi H, Cheng Y, Zhang Q, Hou C, Guan J (2020) Cu nanoparticles embedded in N-doped carbon materials for oxygen reduction reaction, Chinese. *J Chem* 38:941–946. <https://doi.org/10.1002/cjoc.202000073>
 40. Selva G, Araujo TM, Paixao WRLC, Regis T (2015) Non-invasive salivary electrochemical quantification of paraquat poisoning using boron doped diamond electrode. *Electroanal* 27:1642–1648. <https://doi.org/10.1002/elan.201400745>
 41. Zhou M, Tang T, Qin D, Cheng H, Wang X, Chen J, Wågberg T, Hu G (2023) Hematite nanoparticle decorated MIL-100 for the highly selective and sensitive electrochemical detection of trace-level paraquat in milk and honey. *Sensor Actuat B-Chem* 376. <https://doi.org/10.1016/j.snb.2022.132931>
 42. Sant'Anna MVS, Silva JOS, Gevaerd A, Lima LS, Monteiro MDS, Carregosa ISC, Wisniewski A Jr, Marcolino-Junior LH, Bergamini MF, Sussuchi EM (2022) Selective carbonaceous-based (nano)composite sensors for electrochemical determination of paraquat in food samples. *Food Chem* 373:131521. <https://doi.org/10.1016/j.foodchem.2021.131521>
 43. Sun J, Guo F, Shi Q, Wu H, Sun Y, Chen M, Diao G (2019) Electrochemical detection of paraquat based on silver nanoparticles/water-soluble pillar[5]arene functionalized graphene oxide modified glassy carbon electrode. *J Electroanal Chem* 847:113221. <https://doi.org/10.1016/j.jelechem.2019.113221>
 44. Li J, Lei W, Xu Y, Zhang Y, Xia M, Wang F (2015) Fabrication of polypyrrole-grafted nitrogen-doped graphene and its application for electrochemical detection of paraquat. *Electrochim Acta* 174:464–471. <https://doi.org/10.1016/j.electacta.2015.06.028>
 45. Wiwasuku T, Chuaephon A, Habarakada U, Boonmak J, Puangmali T, Kielar F, Harding DJ, Youngme S (2022) A water-stable lanthanide-based MOF as a highly sensitive sensor for the selective detection of paraquat in agricultural products. *ACS Sustain. Chem Eng* 10:2761–2771. <https://doi.org/10.1021/acssuschemeng.1c07966>
 46. Franco DSP, Georgin J, Lima EC, Silva LFO (2022) Advances made in removing paraquat herbicide by adsorption technology: a review. *J Water Process Eng* 49. <https://doi.org/10.1016/j.jwpe.2022.102988>

Publisher's note Springer Nature remains neutral with regard to jurisdictional claims in published maps and institutional affiliations.

Springer Nature or its licensor (e.g. a society or other partner) holds exclusive rights to this article under a publishing agreement with the author(s) or other rightsholder(s); author self-archiving of the accepted manuscript version of this article is solely governed by the terms of such publishing agreement and applicable law.